

# On the Mechanism of the Primary Charge Separation in Bacterial Photosynthesis

C.H. Mak

Department of Chemistry, University of Southern California, Los Angeles, California 90089-0482, USA

Reinhold Egger

Fakultät für Physik, Universität Freiburg, Hermann-Herder-Str. 3, D-79104 Freiburg, Germany

(Date: October 31, 2018)

We present a detailed analysis of the mechanism of the primary charge separation process in bacterial photosynthesis using real-time path integrals. Direct computer simulations as well as an approximate analytical theory have been employed to map out the dynamics of the charge separation process in many regions of the parameter space relevant to bacterial photosynthesis. Two distinct parameter regions, one characteristic of sequential transfer and the other characteristic of superexchange, have been found to yield charge separation dynamics in agreement with experiments. Nonadiabatic theory provides accurate rate estimates for low-lying and very high-lying bacteriochlorophyll state energies, but it breaks down in between these two regimes.

## I. INTRODUCTION

The problem of bacterial photosynthesis has attracted a lot of recent interest since the structures of the photosynthetic reaction center (RC) in purple bacteria *Rhodopseudomonas viridis* and *Rhodobacterias sphaeroides* have been determined [1]. Much research effort is now focused on understanding the relationship between the function of the RC and its structure. One fundamental theoretical question concerns the actual mechanism of the primary electron transfer (ET) process in the RC, and two possible mechanisms (or a combination of both) have emerged out of the recent theoretical work [2–8]. The first is an incoherent two-step mechanism where the charge separation involves a sequential transfer from the excited special pair ( $P^*$ ) via an intermediate bacteriochlorophyll monomer (B) to the bacteriopheophytin (H). The other is a coherent one-step superexchange mechanism, with  $P^+B^-$  acting only as a virtual intermediate.

From experimental studies to date, one cannot easily rule out either possibility. In fact, conflicting interpretations have been derived from different experiments. The detection of transient population in the  $P^+B^-$  state has been considered by many to be the key experimental evidence that can differentiate between the two mechanisms. Many transient absorption spectroscopic experiments [9,10] could not detect bleaching in the  $B^-$  band, lending support to the coherent superexchange mechanism. On the other hand, some other experiments [11,12] point toward a two-step process since a fast second rate constant corresponding to the  $P^+B^-H \rightarrow P^+BH^-$  transition was detected. The picture emerging from a comparison of the molecular dynamics (MD) simulations for the RC carried out so far [13–15] is equally murky. Different groups arrive at conflicting conclusions.

Despite the emphasis placed on the experimental detection of population in the  $P^+B^-$  band, we have shown in a recent real-time path integral simulation [16] that observation of transient population in  $P^+B^-$  cannot definitively rule out either mechanism. In fact, significant population in the  $P^+B^-$  state (up to 20%) can be observed in both the sequential and the superexchange regimes in the simulations. This suggests that transient population on the  $P^+B^-$  state, even if detectable, may not really be useful for differentiating between the two mechanisms [7]. In fact, almost all experimentally observed dynamical features of the RC can be reproduced nicely in either regime.

In this Letter, we report a detailed path integral analysis of the mechanism of the primary charge separation process. We have computed the dynamics of the primary ET (i.e., the time-dependence of the occupation probabilities on the three relevant chromophores) as a function of the  $P^+B^-$  energy for many combinations of the electronic coupling and the reorganization energy. The primary objective is to determine the parameter values that are required for the dynamics to be consistent with characteristic experimental observations, and hence to provide a map of the various possible parameter regions in which the RC could operate. Our previous simulations have been carried out for a relatively small energy range for the  $P^+B^-$  state (between  $-666\text{ cm}^{-1}$  and  $+666\text{ cm}^{-1}$  relative to the  $P^*$  state). In this Letter, we present new results for a much larger range of energies, up to  $3000\text{ cm}^{-1}$  above and  $1333\text{ cm}^{-1}$  below the  $P^*$  state. This spans the region usually considered to be relevant for the RC, except for the region with extremely high  $P^+B^-$  energy (a value of  $+8000\text{ cm}^{-1}$  has been suggested in Ref. [13]).

## II. THREE-STATE SPIN-BOSON MODEL FOR THE RC

The model for our studies has been discussed previously in great detail [8,13,16]. For the sake of completeness, we will summarize some of the relevant features here. For a model of the RC, we consider Hamiltonians of the form

$$H = H_0 + H_B + H_I, \quad (1)$$

where  $H_0$  describes the bare three-state system,  $H_B$  corresponds to a Gaussian bath describing the protein environment, and  $H_I$  is a bilinear system-environment coupling describing the interaction of the electric dipole moment with the bath polarization. The states 1, 2, and 3 correspond to the electronic configurations  $P^*BH$ ,  $P^+B^-H$  and  $P^+BH^-$ , respectively, and we allow for arbitrary binding energies of these states. The bare three-state Hamiltonian is

$$H_0 = \begin{pmatrix} E_1 & -K_{12} & -K_{13} \\ -K_{12} & E_2 & -K_{23} \\ -K_{13} & -K_{23} & E_3 \end{pmatrix}, \quad (2)$$

where the electronic coupling (tunnel matrix element) between states  $i$  and  $j$  is denoted by  $K_{ij}$ .

This spin-boson model is an idealized model for the RC. Its limitations have been discussed in Ref. [16]. The most significant aspect of this model, however, is its ability to capture the effects of the low-frequency protein modes on the tunneling electron from first principles [17]. In this sense, the protein casing in the RC presents itself to the electron as a Gaussian fluctuating polarization field with a continuous spectral density. Previous MD simulations have shown that this spectral density is smooth, featureless, and of Ohmic form with a characteristic frequency  $\omega_c$  of about  $160 \text{ cm}^{-1}$ . They have also confirmed the assumption of Gaussian statistics for the bath polarization since the free energy curves were always found to be strictly parabolic. In the classical (high temperature) limit, the spectral density has a simple relationship with the familiar reorganization energy  $\lambda_{13}$  between states 1 and 3, and one can characterize the Ohmic spectral density completely by the two parameters  $\omega_c$  and  $\lambda_{13}$ . We fix a number of parameters in our model according to reasonable experimental and theoretical estimates [16]:

1. With the energy scale fixed by setting  $E_1 = 0$ , the energy of the  $P^+H^-$  state  $E_3$  is set at  $-2000 \text{ cm}^{-1}$ .
2. The bath frequency  $\omega_c$  is set at  $166 \text{ cm}^{-1}$  according to MD results.
3. The ratio  $K_{23}/K_{12}$  is set at 4, and  $K_{13}$  is assumed to be negligible. All electronic couplings are assumed to be independent of the actual protein configuration (Condon approximation).

The technical details of our real-time quantum Monte Carlo (QMC) simulations have been reported in great detail elsewhere [16] and will not be repeated here. This numerical technique allows for a computation of the time-dependent occupation probabilities on the electronic states up to a certain time limit. QMC simulations cannot be carried out to very long times due to the well-known dynamical sign problem. However, the simulations reported here have been carried out up to a few picoseconds, the same timescale as the experimentally determined ET rate. In these simulations, we search for parameter regions in which the charge separation proceeds in qualitative agreement with experimental observations. We consider the following to be key experimental characteristics: (1) the  $P^+B^-$  population ( $P_2$ ) should be small throughout ( $\lesssim 20\%$ ); (2) the charge separation rate should be about 3 ps at room temperature; and (3) the rate should increase about twofold at cryogenic temperatures. For each value of the  $P^+B^-$  state energy  $E_2$ , we attempt to find a combination of  $K_{12}$  and  $\lambda_{13}$  that would yield dynamics with these experimental characteristics.

## III. QMC SIMULATION RESULTS AND PHASE DIAGRAM

From the QMC simulations, we have compiled a “phase diagram” for the RC, which is a map of the various regions in parameter space which generate dynamics with all the key experimental characteristics. This phase diagram is shown in Fig. 1, with the proper values of  $K_{12}$  correlated with the energy of the  $P^+B^-$  state  $E_2$ . On the phase diagram, we have also indicated the values of  $K_{12}$  predicted by conventional nonadiabatic theory to give a room-temperature ET rate of 3 ps (without demanding that they also conform to the inverse temperature dependence).

From the phase diagram, there are clearly two distinct regions which yield charge separation dynamics with the correct experimental characteristics. The first is characterized by a  $P^+B^-$  state energy  $E_2$  lower than about  $-600 \text{ cm}^{-1}$  and down to about  $-1300 \text{ cm}^{-1}$ . Within this region, the dynamics largely agrees with predictions from conventional nonadiabatic theory for the sequential mechanism. Simulation results for the transient populations on the three electronic states are shown in Fig. 2 at two temperatures for  $E_2 = -666 \text{ cm}^{-1}$  and  $-1333 \text{ cm}^{-1}$ . The  $1 \rightarrow 3$  transfer is efficient in both cases, with  $P_2$  remaining below 15% throughout. For  $E_2 = -666 \text{ cm}^{-1}$ , the charge separation rate increases from 3.0 ps at 298 K to 2.0 ps at 140 K. This should be contrasted with  $E_2 = -1333 \text{ cm}^{-1}$ , for which the rate increases from 3.3 ps at 298 K to only 2.7 ps at 140 K. Although the ET rate still increases with lower temperature for  $E_2 = -1333 \text{ cm}^{-1}$ , this temperature-dependence is somewhat weaker than that observed in experiments. For  $E_2$  much below  $-1333 \text{ cm}^{-1}$ , the temperature depen-

dence is not strong enough to be consistent with experiments. Therefore, in the phase diagram, the sequential region terminates around  $E_2 = -1333 \text{ cm}^{-1}$ .

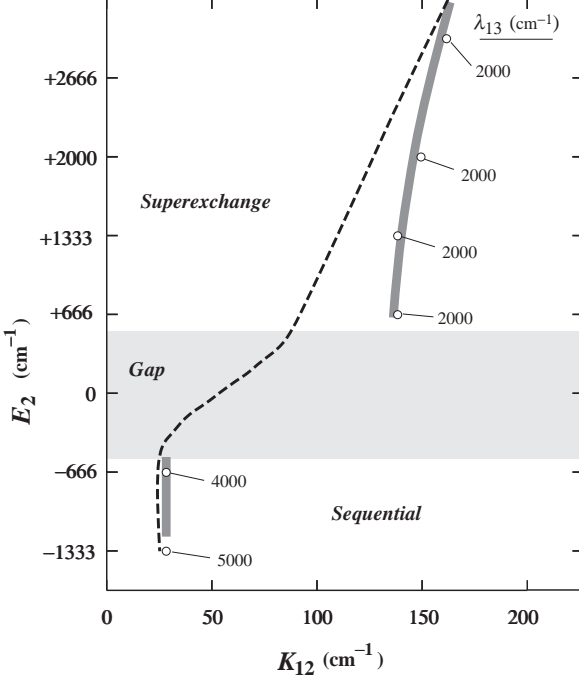


FIG. 1. Phase diagram of the RC compiled from QMC simulation data, correlating  $K_{12}$  with  $E_2$  (thick lines). The proper reorganization energies are indicated on the phase diagram for those parameter sets that yield dynamics consistent with experiments (open circles). Nonadiabatic predictions for the  $K_{12}$  yielding a room-temperature rate of 3 ps are also shown for comparison (dashed curve).

The second region is characterized by a  $\text{P}^+\text{B}^-$  state energy  $E_2$  higher than  $+666 \text{ cm}^{-1}$  (we have performed simulations for  $E_2$  up to  $+3000 \text{ cm}^{-1}$ ). For  $E_2 = +666 \text{ cm}^{-1}$  and  $+1333 \text{ cm}^{-1}$ , conventional nonadiabatic superexchange theory does *not* give reliable predictions for the dynamics. The transfer mechanism in this region is predominantly superexchange, although the precise rates are not well described by nonadiabatic theory. As the energy of the  $\text{P}^+\text{B}^-$  state moves up to  $E_2 = +2000 \text{ cm}^{-1}$  and beyond, the dynamics becomes increasingly nonadiabatic. We mention in passing that in this limit the dynamical sign problem is quite severe, and one needs to sample extremely long Monte Carlo trajectories rendering QMC simulations for  $E_2$  much higher than  $+3000 \text{ cm}^{-1}$  very costly. Nevertheless, our present data show that for sufficiently high-lying  $\text{P}^+\text{B}^-$  state, the conventional golden rule superexchange formula becomes increasingly accurate, making QMC simulations less valuable for  $E_2 > +3000 \text{ cm}^{-1}$ . For  $E_2 < +2000 \text{ cm}^{-1}$ , however, nonadiabatic theory seems to severely underestimate the mag-

nitude of the electronic couplings required to achieve superexchange rates consistent with experiments.

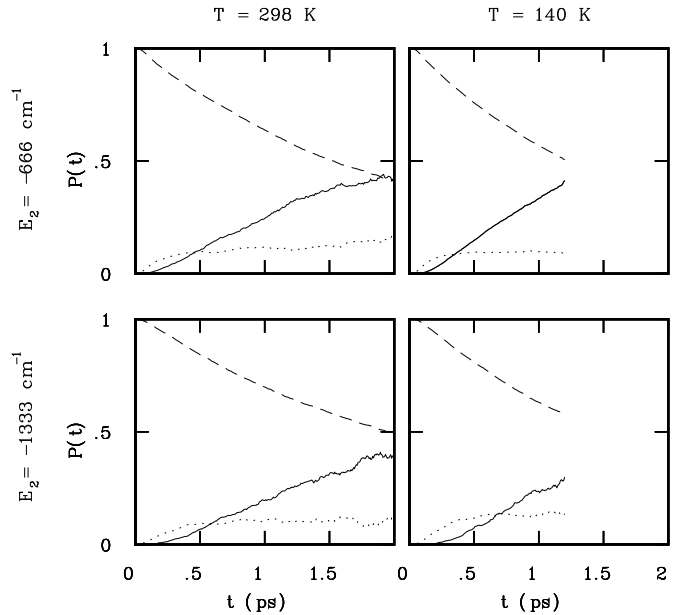


FIG. 2. QMC data for the ET dynamics with low-lying  $\text{P}^+\text{B}^-$  state and  $K_{12} = 28 \text{ cm}^{-1}$  for  $E_2 = -666 \text{ cm}^{-1}$  ( $\lambda_{13} = 4000 \text{ cm}^{-1}$ ) and  $E_2 = -1333 \text{ cm}^{-1}$  ( $\lambda_{13} = 5300 \text{ cm}^{-1}$ ). The dashed (dotted, solid) curve gives the occupation probability on state 1 (2, 3).

Simulation results for the transient populations on the three electronic states are shown in Fig. 3 at two temperatures for  $E_2 = +666 \text{ cm}^{-1}$ ,  $+1333 \text{ cm}^{-1}$  and  $+2000 \text{ cm}^{-1}$ . For all three energies, the charge separation rates at 298 K are about 3 ps. These rates increase to about 2.2 to 2.5 ps at 140 K. As was pointed out in our previous work [16], the dynamics in this regime is not simply monoexponential. There is a fast short-time component for the first  $\approx 0.5$  ps, followed by a slower component. The fast component always obeys the experimentally observed inverse temperature dependence, but the rate and the proportion of the slower component vary nonmonotonically with temperature, as measured in many mutant RCs [18]. The physical reason for this phenomenon has been given by Gehlen et al. [19], and our simulations provide direct numerical support for their arguments.

The phase diagram in Fig. 1 also reveals another interesting aspect of the superexchange regime: the RC seems to be able to operate under a wide range of  $\text{P}^+\text{B}^-$  state energies with the same conditions, i.e., with approximately the same electronic coupling  $K_{12}$  (about 140 to  $150 \text{ cm}^{-1}$ ) and the same reorganization energy  $\lambda_{13}$  (about  $2000 \text{ cm}^{-1}$ ). This means that within the superexchange regime, the system is robust against variation in the  $\text{P}^+\text{B}^-$  state energy. The sequential region is not as robust. Although approximately the same value of

$K_{12}$  (about  $28 \text{ cm}^{-1}$ ) would work for  $E_2$  between about  $-1333 \text{ cm}^{-1}$  and  $-666 \text{ cm}^{-1}$ , the optimal value of the reorganization energy  $\lambda_{13}$  changes from  $4000 \text{ cm}^{-1}$  at  $E_2 = -666 \text{ cm}^{-1}$  to  $5300 \text{ cm}^{-1}$  at  $E_2 = -1333 \text{ cm}^{-1}$ .

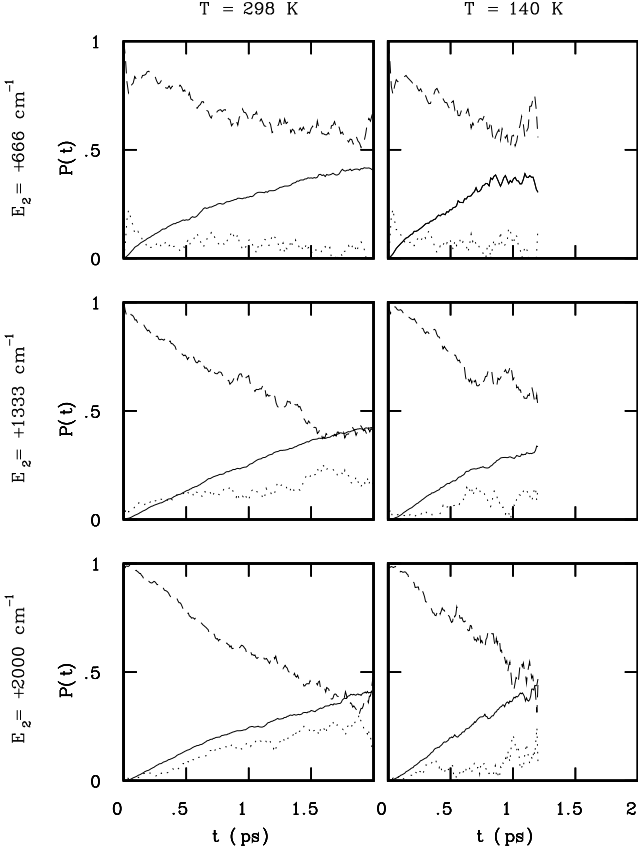


FIG. 3. QMC data for high-lying  $\text{P}^+\text{B}^-$  state with  $\lambda_{13} = 2000 \text{ cm}^{-1}$ . The couplings are  $K_{12} = 140 \text{ cm}^{-1}$  for  $E_2 = +666, +1333 \text{ cm}^{-1}$ , and  $K_{12} = 150 \text{ cm}^{-1}$  for  $E_2 = +2000 \text{ cm}^{-1}$ .

Finally, it is important to stress that the RC does *not* seem to operate via a combined sequential/superexchange mechanism as proposed in Refs. [4,20]. Our simulations indicate clearly that it is either a pure sequential or a pure superexchange transfer. This is indicated by the grey region in Fig. 1, which we refer to as the “gap” region. We emphasize that this does not imply that in this region it is impossible to achieve a fast ET rate. On the contrary, it is possible to achieve a 3 ps transfer at room temperature with only minor population accumulation on the  $\text{P}^+\text{B}^-$  state. However, we have not found any parameter set in this region that can simultaneously satisfy all the experimentally observed characteristics *both* at high and low temperatures [16].

#### IV. NONINTERACTING-CLUSTER APPROXIMATION

By invoking a simple and reasonable approximation for the formally exact path-integral expressions, we have previously derived a set of nonlocal master equations for the time-dependent occupation probabilities [8]. Our “noninteracting-cluster approximation” (NICA) expresses the time-dependent transition rates between the various sites in terms of cluster functions  $\Gamma_{ij}$ . These cluster functions give the amplitude of all paths going from diagonal state  $i$  to diagonal state  $j$  of the reduced density matrix without touching the diagonal in between. Since each hop on the  $3 \times 3$  lattice representing the possible states of the reduced density matrix gives a factor  $\pm iK_{ij}$ , the rates can be expressed as a power series in the electronic couplings.

By confining this expansion to the lowest-order terms and taking the long-time limit (which makes the master equations local in time), one obtains the nonadiabatic rate expressions referred to in Sec. III. The rates  $\Gamma_{12}$  and  $\Gamma_{23}$  (plus backward rates) describing a sequential transfer are just golden rule rates. Furthermore, the lowest-order cluster  $\Gamma_{13}^{(4)} \sim K_{12}^2 K_{23}^2$  gives the nonadiabatic superexchange rate. There is only one pathway contributing to this fourth-order cluster (plus the complex conjugate), namely the one going along the edge of the  $3 \times 3$  lattice. The resulting rate formula can be further simplified in the classical limit by taking a short-time approximation for the bath kernel, or for a high-lying state where one can derive the conventional golden rule rate for the emerging two-state system spanned by states 1 and 3 [8]. These golden rule rates are consistent with the QMC results for very high  $\text{P}^+\text{B}^-$  state energy ( $E_2 \gtrsim +2000 \text{ cm}^{-1}$ ) as well as for low-lying  $\text{P}^+\text{B}^-$  states ( $E_2 \lesssim -666 \text{ cm}^{-1}$ ). But in the intermediate region  $+666 \text{ cm}^{-1} \lesssim E_2 \lesssim +2000 \text{ cm}^{-1}$ , nonadiabatic theory breaks down (see Fig. 1).

We will now study the origin of the apparent discrepancy between nonadiabatic theory and the QMC results in this intermediate region. To that purpose, we have computed the next-order corrections to the superexchange cluster,  $\Gamma_{13}^{(6)}$ . Here one has to consider the two pathways with six hops which go from diagonal state 1 to state 3 without hitting the diagonal. In the classical limit, we obtain for the activationless situation considered in the simulations ( $E_3 = -\lambda_{13}$ )

$$\frac{\Gamma_{13}^{(6)}}{\Gamma_{13}^{(4)}} = -\frac{K_{12}^2 + K_{23}^2}{4(\delta E)^2} \left( 1 - \frac{2\beta F^*}{1 + \exp(\beta F^*)} \right), \quad (3)$$

where  $\delta E = E_2 + \lambda_{13}/4$  and  $F^* = (\delta E)^2/\lambda_{13}$ . For a high-lying intermediate state, the bracket gives unity because  $\beta F^* \gg 1$ . Therefore the sixth-order correction decreases the nonadiabatic estimate by  $\approx 20\%$  for  $E_2 = +666 \text{ cm}^{-1}$ . With the short-time bath kernel, it would actually be possible to sum the whole power series and thus to obtain the full classical NICA superexchange

rate without stopping at sixth order. However, we have not done so because this short-time approximation is inappropriate for high-order diagrams. In any case, it is expected that these higher-order contributions lead to a *reduction* of the nonadiabatic superexchange rate. Moreover, we also expect that adiabatic corrections beyond NICA can lead to substantial renormalizations for large electronic couplings.

To conclude, we have given a path-integral analysis of the primary electron transfer step in bacterial photosynthesis. The mechanism appears to be either a sequential or a superexchange transfer but not a combined one. Whereas conventional nonadiabatic theory appears to be accurate for both the sequential and the ultimate superexchange regime, adiabatic corrections reduce the superexchange rate substantially for intermediate energies of the  $P^+B^-$  state.

We wish to thank David Chandler and Uli Weiss for illuminating discussions. This work was supported in part by the National Science Foundation (CHE-9216221) and the NSF Young Investigator Awards Program (CHE-9257094), the Camille and Henry Dreyfus Foundation under the Camille Teacher-Scholar Award Program, and the Sloan Foundation through a Alfred P. Sloan Fellowship. Computational resources from IBM are acknowledged.

- [12] K. Dressler, E. Umlauf, S. Schmidt, P. Hamm, W. Zinth, S. Buchanan and H. Michel, *Chem. Phys. Lett.* 183 (1991) 270.
- [13] M. Marchi, J.N. Gehlen, D. Chandler and M. Newton, *J. Am. Chem. Soc.* 115 (1993) 4178.
- [14] S. Creighton, J.K. Hwang, A. Warshel, W.W. Parson and J. Norris, *Biochemistry* 27 (1988) 774; A. Warshel and W.W. Parson, *Ann. Rev. Phys. Chem.* 42 (1991) 279.
- [15] K. Schulten and M. Tesch, *Chem. Phys.* 158 (1991) 421.
- [16] R. Egger and C.H. Mak, *J. Phys. Chem.* 98 (1994) 9903. The QMC algorithm is described in more detail in: R. Egger and C.H. Mak, *Phys. Rev. B* (in press).
- [17] A.J. Leggett, S. Chakravarty, A.T. Dorsey, M.P.A. Fisher, A. Garg and W. Zwerger, *Rev. Mod. Phys.* 59 (1987) 1; U. Weiss, *Quantum Dissipative Systems* (World Scientific, Singapore, 1993).
- [18] M. Du, S.J. Rosenthal, X. Xie, T.J. DiMagno, M. Schmidt, D.K. Hanson, M. Schiffer, J.R. Norris, and G.R. Fleming, *Proc. Natl. Acad. Sci. USA* 89 (1992) 8517; Y. Jai, T.J. DiMagno, C.K. Chan, Z. Wang, M. Du, D.K. Hanson, M. Schiffer, J.R. Norris, G.R. Fleming and M.S. Popov, *J. Phys. Chem.* 97 (1993) 13180.
- [19] J.N. Gehlen, M. Marchi and D. Chandler, *Science* 263 (1994) 499.
- [20] C.K. Chan, T.J. DiMagno, L.X.Q. Chen, J.R. Norris and G.R. Fleming, *Proc. Natl. Acad. Sci. USA* 88 (1991) 11202.

---

- [1] J. Deisenhofer, O. Epp, K. Miki, R. Huber and H. Michel, *J. Mol. Biol.* 180 (1984) 385; J.P. Allen, G. Feher, T.O. Yeates, H. Komiya and D.C. Rees, *Proc. Natl. Acad. Sci. USA* 84 (1987) 5730; C.H. Chang, D.M. Tiede, J. Tang, U. Smith, J.R. Norris and M. Schiffer, *FEBS Lett.* 205 (1986) 82.
- [2] R.A. Marcus, *Chem. Phys. Lett.* 133 (1987) 471; *ibid.* 146 (1988) 13.
- [3] M. Bixon, J. Jortner, M.E. Michel-Beyerle, A. Ogrodnik and W. Lersch, *Chem. Phys. Lett.* 140 (1987) 626.
- [4] M. Bixon, J. Jortner and M.E. Michel-Beyerle, *Biochim. Biophys. Acta* 1056 (1991) 301.
- [5] R.A. Marcus and R. Almeida, *J. Phys. Chem.* 94 (1990) 2973; R. Almeida and R.A. Marcus, *ibid.* 94 (1990) 2978.
- [6] Y. Hu and S. Mukamel, *J. Chem. Phys.* 91 (1989) 6973.
- [7] J.S. Joseph and W. Bialek, *J. Phys. Chem.* 97 (1993) 3255; *Biophys. J.* 63 (1992) 397.
- [8] R. Egger, C.H. Mak and U. Weiss, *Phys. Rev. E* 50 (1994) R655.
- [9] J.L. Martin, J. Breton, A.J. Hoff, A. Migus and A. Antonetti, *Proc. Natl. Acad. Sci. USA* 83 (1986) 957; J. Breton, J.L. Martin, G.R. Fleming and J.C. Lambry, *Biochemistry* 27 (1988) 8276.
- [10] C. Kirmaier and D. Holten, *Proc. Natl. Acad. Sci. USA* 87 (1990) 3552; *Biochemistry* 30 (1991) 611.
- [11] W. Holzapfel, U. Finkele, W. Kaiser, D. Oesterhelt, H. Scheer, H.U. Stilz and W. Zinth, *Chem. Phys. Lett.* 160 (1989) 1; *Proc. Natl. Acad. Sci. USA* 87 (1990) 5168.